Discontinuous Hall coefficient at the quantum critical point in $YbRh_2Si_2$

2011 J. Phys.: Condens. Matter 23 094216

(http://iopscience.iop.org/0953-8984/23/9/094216)

IOP Publishing Journal of Physics: Condensed Matter

J. Phys.: Condens. Matter **23** (2011) 094216 (8pp) doi:10.1088/0953-8984/23/9/094216

Discontinuous Hall coefficient at the quantum critical point in $YbRh_2Si_2$

Sven Friedemann[1,5], Niels Oeschler[1], Steffen Wirth[1], Cornelius Krellner[1], Christoph Geibel[1], Frank Steglich[1], Silke Paschen[2], Stefan Kirchner[3,4] and Qimiao Si[3]

[1] Max Planck Institute for Chemical Physics of Solids, Nöthnitzer Straße 40, 01187 Dresden, Germany

[2] Institute of Solid State Physics, TU Vienna, Wiedner Hauptstrasse 8-10, 1040 Vienna, Austria

[3] Department of Physics and Astronomy, Rice University, Houston, TX 77005, USA

[4] Max Planck Institute for the Physics of Complex Systems, Nöthnitzer Straße 38, 01187 Dresden, Germany

E-mail: Sven.Friedemann@cpfs.mpg.de

Received 15 September 2010, in final form 27 November 2010
Published 17 February 2011
Online at stacks.iop.org/JPhysCM/23/094216

Abstract

$YbRh_2Si_2$ is a model system for quantum criticality. In particular, Hall effect measurements helped identify the unconventional nature of its quantum critical point. Here, we present a high-resolution study of the Hall effect and magnetoresistivity on samples of different quality. We find a robust crossover on top of a sample dependent linear background contribution. Our detailed analysis provides a complete characterization of the crossover in terms of its position, width, and height. Importantly, we find in the extrapolation to zero temperature a discontinuity of the Hall coefficient occurring at the quantum critical point for all samples. In particular, the height of the jump in the Hall coefficient remains finite in the limit of zero temperature. Hence, our data solidify the conclusion of a collapsing Fermi surface. Finally, we contrast our results to the smooth Hall effect evolution seen in chromium, the prototype system for a spin-density-wave quantum critical point.

(Some figures in this article are in colour only in the electronic version)

1. Introduction

A quantum critical point (QCP) marks a continuous phase transition at zero temperature. A non-thermal parameter, such as pressure or magnetic field, is used to tune a material from one state to another. Experimentally, QCPs are often accessed by suppressing a finite temperature phase transition. At zero temperature, quantum effects become dominant. Surprisingly, the quantum fluctuations between the two incompatible ground states lead to a rich variety of phenomena even at finite temperatures. In fact, quantum critical phenomena are believed to be relevant for a large variety of correlated materials, such as quantum magnets, heavy-fermion materials, and even high-temperature superconductors [1].

Heavy-fermion materials play a major role in the study of quantum critical phenomena [2]. These intermetallic compounds appear to be model systems, because two competing interactions leading to two different ground states may be shifted relative to each other allowing one to tune the material from one ground state to another. Both, the Kondo interaction and the Ruderman–Kittel–Kasuya–Yosida (RKKY) interaction arise from the interplay between conduction electrons and magnetic f electrons, the latter being provided by rare earth elements. The Kondo effect marks the screening of f electrons by conduction electrons, leading to composite quasiparticles with largely enhanced effective masses. These quasiparticles arise in the Kondo-screened spin-singlet ground state. Whereas the Kondo effect favors a paramagnetic Landau–Fermi-liquid (LFL) ground state, the RKKY interaction mediates a magnetic exchange between f electrons and, hence, favors long range magnetic

[5] Present address: Cavendish Laboratory, University of Cambridge, JJ Thomson Avenue, Cambridge, CB3 0HE, UK.

order. The different dependences of the Kondo effect and the RKKY interaction on the coupling strength of conduction electrons and f electrons provides the basis for tuning heavy-fermion materials to quantum criticality in a controlled fashion: pressure for instance increases the hybridization of conduction electrons and f moments, hence, increasing the Kondo coupling strength. The Kondo effect dominates in the strong coupling regime, whereas the RKKY interaction dominates in the weak coupling regime. At an intermediate coupling strength, both balance each other such that a magnetic transition arising at weak coupling due to the RKKY interaction is suppressed to zero temperature, giving rise to the QCP.

The conventional description of a QCP is based on the Ginzburg–Landau concept of order parameter fluctuations. It generalizes its counterpart for classical critical points by incorporating the quantum fluctuations. For the metallic heavy-fermion systems the magnetism is treated itinerantly as a spin-density-wave (SDW) [3–5]. Within this picture, the composite quasiparticles are assumed to stay intact at the QCP: they form both the magnetically ordered ground state on one side of the QCP as well as the paramagnetic heavy Fermi liquid on the other side. In addition, the fact that the QCP corresponds to a Gaussian fixed point implies that the fluctuations violate energy over temperature, E/T, scaling [6]. In disagreement with this fundamental property of a conventional QCP, the magnetic fluctuations in $CeCu_{5.9}Au_{0.1}$ were observed to obey an E/T scaling [7]. This stimulated new theoretical approaches.

In unconventional theories of the QCP additional quantum modes are assumed to become critical. These additional critical modes may lead to an interacting fixed point for which the fluctuations satisfy E/T scaling in contrast to the SDW scenario, hence, explaining the observations in $CeCu_{5.9}Au_{0.1}$. For the case of the heavy-fermion materials these additional modes are associated with the breakdown of the Kondo effect [8–10]. As a consequence, the composite quasiparticles are expected to disintegrate at the QCP, leaving the f electrons decoupled from the conduction electron sea on the weak coupling side. Consequently, the Fermi surface is expected to change from 'large', with the f states incorporated on the strong coupling side, to 'small', with the f states decoupled from the conduction electron sea on the weak coupling side. As such a Fermi surface collapse is not expected in the conventional scenario, measurements of the Fermi surface evolution were suggested to unveil the nature of a particular heavy-fermion QCP [8, 9]. In fact, Hall effect measurements gave indications of a discontinuous evolution across the QCP in $YbRh_2Si_2$ [11]. Here, a crossover of the Hall coefficient is observed at finite temperatures. As the temperature is lowered this crossover sharpens. With the width of the crossover vanishing in the extrapolation to zero temperature an abrupt jump of the Hall coefficient at the QCP is suggested. Consequently, these measurements indicate a reconstruction of the Fermi surface at the QCP. However, this Hall effect study was discussed controversially, particularly in view of sample dependences in the low temperature Hall coefficient [12]. The Hall coefficient is extremely sensitive to small changes in the relative scattering rates of the two dominant bands, which almost compensate each other [13]. These changes in the scattering rates seem to originate from tiny variations in the chemical composition, as they only affect samples from different batches.

In order to identify the influence of the sample dependences on the behavior at the QCP, a high-resolution Hall effect study on different samples of $YbRh_2Si_2$ was carried out [14]. This study revealed the crossover in the Hall coefficient to be robust against sample dependences. Moreover, the results gave indications for the electronic fluctuations to obey E/T scaling. Consequently, $YbRh_2Si_2$ seems to be the first material in which both the fundamental signatures of a Kondo breakdown QCP are seen, i.e., the Fermi surface reconstruction and E/T scaling. Given this key role of $YbRh_2Si_2$ for the understanding of quantum critical phenomena, it is important to carefully scrutinize the picture of a Fermi surface reconstruction.

Here, we present extended measurements and a detailed analysis of the magnetotransport properties across the QCP surveying different samples. Our detailed analysis of the data at very low temperatures allows one to establish a proper extrapolation of the characteristics of the Hall coefficient to zero temperature. We show that these characteristics are distinct from the theoretical predictions for a SDW QCP and the experimental observations in the canonical SDW QCP system, chromium.

2. Experimental setup

Pronounced non-Fermi-liquid behavior of $YbRh_2Si_2$, such as a linear temperature dependence of the resistivity and a divergent specific heat, were interpreted in terms of its proximity to a QCP. In zero-field, $YbRh_2Si_2$ orders antiferromagnetically below the Néel temperature $T_N = 70$ mK [15]. The application of a small magnetic field of $B_{c2} = 60$ mT applied perpendicular to the crystallographic c direction, or of $B_{c1} = 660$ mT applied along the crystallographic c axis, suppresses the magnetic order to zero temperature, thus accessing the field induced QCP [16]. For fields exceeding the critical field a paramagnetic LFL ground state is observed.

Single crystals of $YbRh_2Si_2$ were grown in indium flux, as described earlier [15]. By optimizing the growth procedure, the quality of the crystals was advanced. Two different samples were chosen: sample 1 possessing a residual resistivity ratio RRR = 70 was taken from [11]. Sample 2 with RRR = 120 was taken from the highest quality batch available.

We utilize three different magnetotransport techniques to study the Fermi surface evolution of $YbRh_2Si_2$. First, the crossed-field Hall effect geometry is used to measure the linear-response Hall coefficient. Here, two different magnetic fields allow one to disentangle the two responses to the magnetic field (cf inset in figure 1): a small field B_1 oriented along the c direction, and perpendicular to the current I, is used to induce a transverse Hall voltage. A second field B_2 within the ab plane and parallel to the current is used to tune the sample across the QCP. The tuning effect of B_1 is negligible thanks to the magnetic anisotropy, seen for instance in the ratio of the critical fields. The Hall resistivity ρ_H is calculated as the antisymmetric part of the

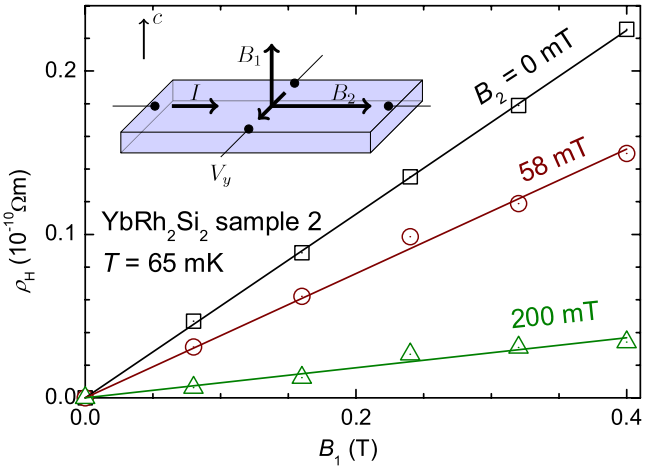

Figure 1. Exemplary Hall resistivity isotherms for sample 2. Solid lines mark linear fits to the data, with the slope of these lines corresponding to the linear-response Hall coefficient R_H. The inset sketches the crossed-field Hall effect setup.

transverse voltage V_y with respect to B_1 in order to separate magnetoresistance contributions, $\rho_H(B_1, B_2) = t/(2I) \times [V_y(B_1, B_2) - V_y(-B_1, B_2)]$. The Hall resistivity obeys a linear field dependence, as displayed in figure 1. The initial-slope Hall coefficient R_H was subsequently numerically extracted as the slope of linear fits to the Hall resistivity

$$R_H(B_2) \equiv \lim_{B_1 \to 0} \frac{\rho_H(B_1, B_2)}{B_1} \tag{1}$$

at fixed tuning field B_2 for Hall fields $B_1 \leqslant 0.4$ T. Consequently, the decrease of the slope in $\rho_H(B_1)$ as the field B_2 is increased, as seen in figure 1, corresponds to a decrease of the Hall coefficient. Second, the results are corroborated by measurements in the standard single-field setup. Here, only the magnetic field B_1 (parallel to c) is used to perform both tasks of tuning the sample and generating the Hall response. By analyzing the differential Hall coefficient

$$\tilde{R}_H(B_1) = \frac{\partial \rho_H(B_1, 0)}{\partial B_1} \tag{2}$$

we subsequently disentangle these two effects. Third, longitudinal magnetoresistivity with current flowing in the ab plane was monitored over an extended temperature range and provides increased statistics.

For the electrical transport measurements, rectangular platelets with a thickness t between 25 and 80 μm were used. Spot-welded gold wires provided contacts with resistances well below 1 Ω. An alternating current I up to 100 μA flowed within the ab plane. Voltages arising from magnetoresistance and the Hall effect were amplified with low temperature transformers and subsequently monitored via a standard lock-in technique. For $YbRh_2Si_2$, the anomalous contributions to the Hall coefficient [17] are negligible at low temperatures [18, 14].

3. Results and discussion

Low temperature isotherms of the linear-response Hall coefficient as a function of B_2 are displayed in figure 2. Both samples show a similar qualitative behavior consisting of two features: at small fields, the Hall coefficient decreases in a pronounced crossover, and at higher fields and low temperatures this crossover is succeeded by a linear increase. The crossover was already earlier recognized as being part of the intrinsic quantum critical behavior [11], whereas the linear increase is only apparent in the extended field and temperature range studied here. Both the crossover and the linear high-field behavior obey temperature dependences: the crossover in $R_H(B_2)$ is shifted towards smaller fields approaching the QCP and becomes sharper as the temperature is lowered. Hence, the linear behavior is revealed over an increasing field range as the temperature is lowered. This suggests that the linear behavior represents a background contribution that presumably originates from Zeeman splitting. The slope of this background contribution is reduced above 100 mK and becomes slightly negative for sample 1 at 300 mK. Despite the robust characteristics of the curves, the absolute values of the Hall coefficient differ for the two samples. This is in accordance to the above mentioned sample dependences.

Differential Hall coefficient and magnetoresistivity are depicted in figure 3 for both samples. As in the linear-

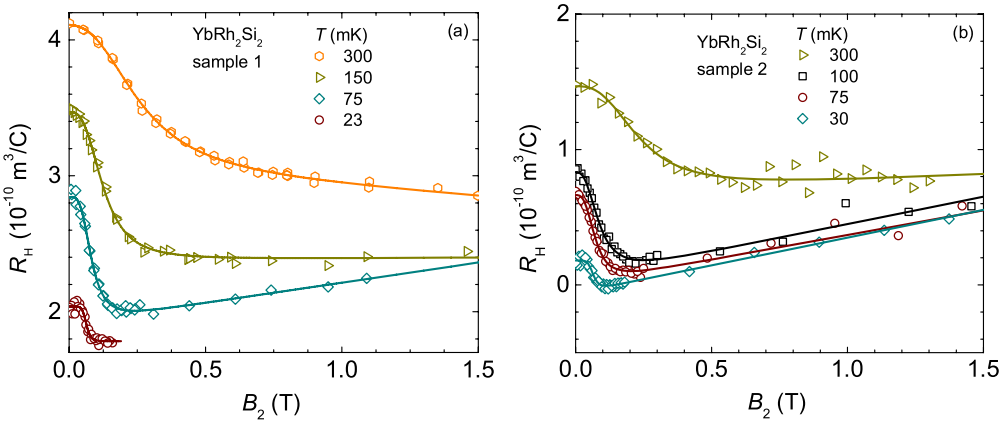

Figure 2. Field dependence of the initial-slope Hall coefficient, $R_H(B_2)$, for sample 1 (a) and 2 (b). Sample 1 was taken from [11]. Solid lines represent fits of equation (3) to the data.

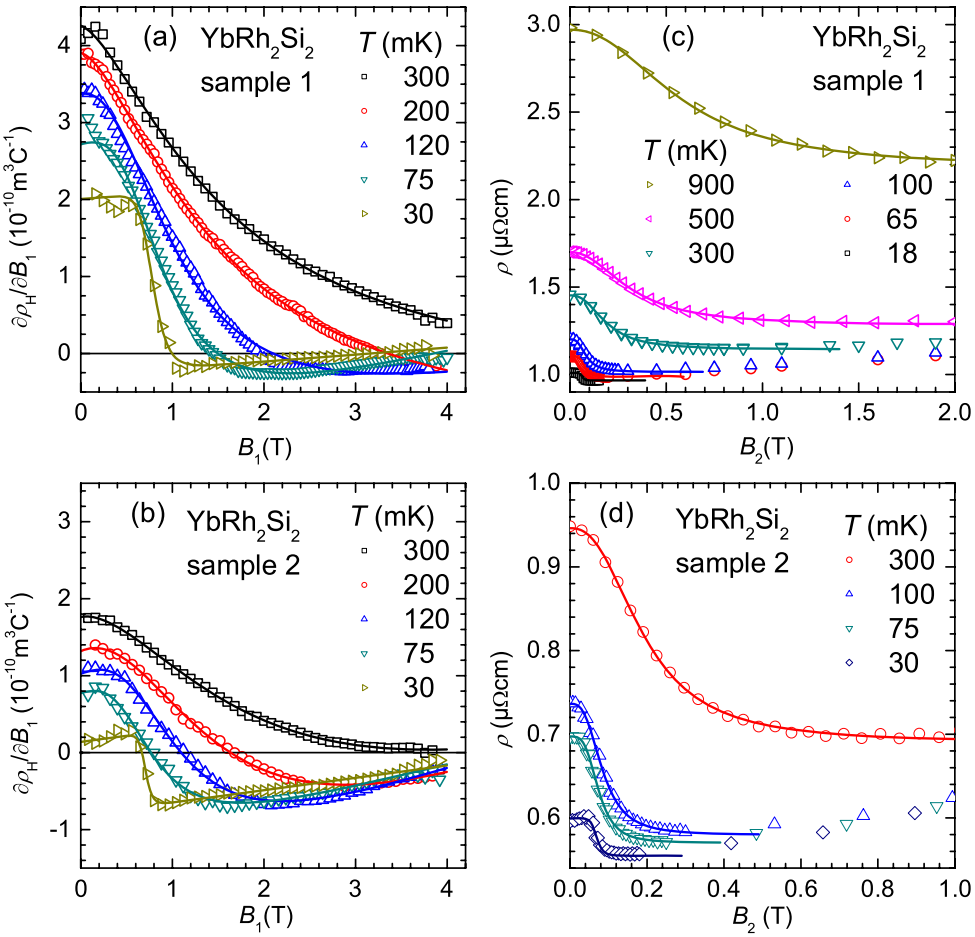

Figure 3. Differential Hall coefficient (left) and magnetoresistivity (right) isotherms of sample 1 (upper panels) and sample 2 (lower panels). Solid lines mark fits of equation (3) to the data. In the case of the magnetoresistivity the linear term ($m = 0$) was omitted, as it better describes the data.

response Hall coefficient, we can identify a crossover and a linear background contribution. Again, the crossover shifts to smaller fields and becomes sharper as the temperature is lowered. Also, a decrease of the crossover height is seen in both differential Hall coefficient and magnetoresistivity. Nevertheless, the absolute height of the crossover in the differential Hall coefficient is larger compared to the linear-response Hall coefficient. Finally, the signatures are seen in both samples, with the absolute values varying according to the sample dependences of the Hall coefficient and the different residual resistivity of the samples, respectively.

The presence of the crossover in both samples and in various transport properties suggests that this signature of the QCP is not affected by sample dependences. Rather, the sample dependences seem to be exclusively related to the background contribution [13]. In order to check this we shall quantitatively analyze the crossover for its position and width. In addition, our high-resolution study over an extended temperature range reveals the height of the crossover to become smaller with decreasing temperature. This motivates a careful analysis of the limiting parameters of the Hall crossover in order to check if the change of the Hall coefficient is retained at the QCP, i.e., in the extrapolation to zero temperature. In order to scrutinize this, we analyze the Hall coefficient by fitting the empirical crossover function

$$R_{\mathrm{H}}(B_2) = R_{\mathrm{H}}^{\infty} + mB_2 - \frac{R_{\mathrm{H}}^{\infty} - R_{\mathrm{H}}^{0}}{1 + (B_2/B_0)^p} \qquad (3)$$

to the data. Here, R_{H}^{0} and R_{H}^{∞} parametrize the zero-field and high-field value, respectively. The position of the crossover is represented by B_0 and its sharpness is determined by p. The superposed linear term mB_2 is added to reflect the background behavior. Analogous fitting procedures lead to the zero-field and high-field values of the single-field Hall experiment ($\tilde{R}_{\mathrm{H}}^{0}$ and $\tilde{R}_{\mathrm{H}}^{\infty}$) and of the magnetoresistivity experiment (ρ^0 and ρ^{∞}), respectively. Equation (3) allows us to analyze the characteristics of the crossover separately from the linear background.

First, we examine the position of the crossover. Figure 4 depicts the crossover field B_0 extracted from the three experiments and for both samples in the low temperature–magnetic field phase diagram. We note that in the case of the single-field Hall experiment, the magnetic anisotropy ratio $B_{c2}/B_{c1} = 1/11$ is used to convert the results to an equivalent B_2 scale. For both samples and the complete set of experiments, B_0 is seen to shift to lower fields as the temperature is decreased. In the limit of zero temperature it

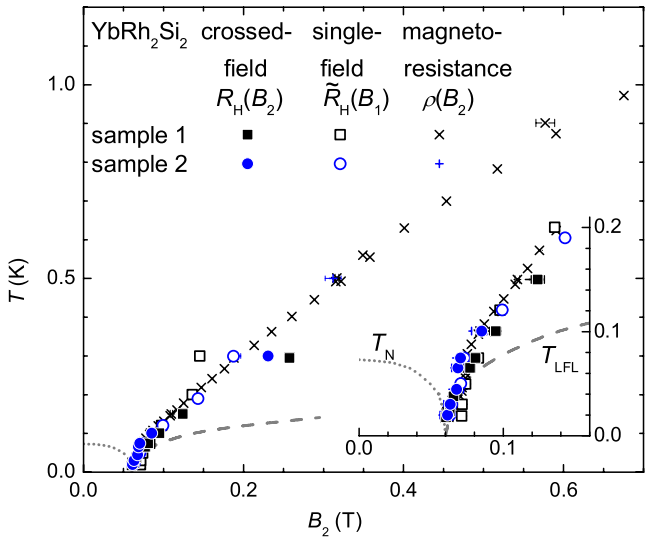

Figure 4. Position of the crossover fields from the Hall effect $R_H(B_2)$ and $\tilde{R}_H(B_1)$ and magnetoresistivity $\rho(B_2)$ in the magnetic field–temperature phase diagram (cf figures 2 and 3). Single-field results are scaled by $B_{c2}/B_{c1} = 1/11$, accounting for the magnetic anisotropy of $YbRh_2Si_2$ [16]. The inset magnifies the low temperature range. Dotted and dashed lines respectively represent the boundary of the magnetically ordered state and the boundary of the regime with LFL behavior as deduced from resistivity measurements [16].

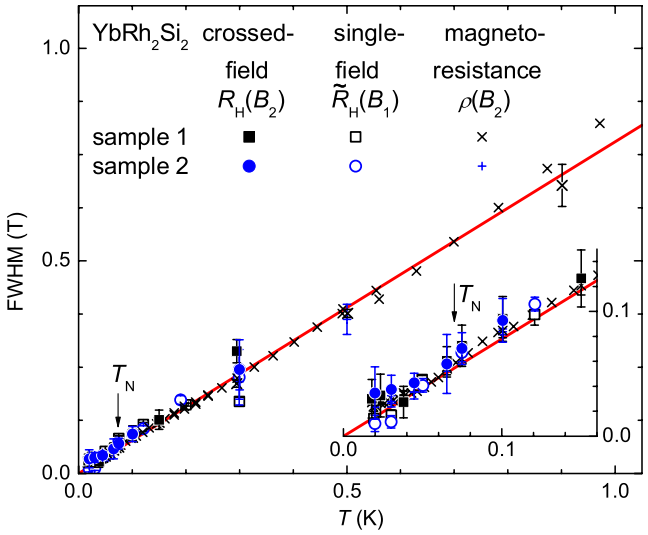

Figure 5. Full width at half maximum (FWHM) of the crossovers in the Hall coefficient and magnetoresistivity. Single-field results are scaled by $B_{c2}/B_{c1} = 1/11$. The FWHM was extracted from the derivative of equation (3) fitted to the linear-response Hall coefficient $R_H(B_2)$, differential Hall coefficient $\tilde{R}_H(B_1)$, and magnetoresistivity $\rho(B_2)$ (cf figures 2 and 3). The solid line represents a linear fit to all data sets. Within the error this line intersects the origin. The inset magnifies data at the lowest temperatures. The arrow indicates the Néel temperature.

extrapolates to 60 mT, i.e., to the QCP as illustrated in the inset of figure 4. This emphasizes the robust assignment of the crossover to quantum criticality.

Second, in order to quantify the width of the crossover the derivative of the fitted function is analyzed. The crossover in $R_H(B_2)$ corresponds to a (negative) peak in the derivative dR_H/dB_2 and analogously in $d\tilde{R}_H/dB_1$ and $d\rho/dB_2$. We examine the full width at half maximum (FWHM) of this peak as plotted in figure 5. The analysis reveals that also the width of the crossover is unaffected by the sample dependences: within the experimental resolution the data of the two samples match. Moreover, the different experiments yield identical results within experimental accuracy. The FWHM decreases as the temperature is lowered. Importantly, FWHM(T) is best described by a proportionality to temperature extrapolating to zero for $T = 0$. In fact, no signature is seen at the Néel temperature, in contrast to the height of the crossover discussed below. At temperatures below 30 mK the crossed-field data show a slight trend towards saturation, which is however absent in the single-field data. This might indicate that the classical fluctuations play a role at these lowest temperatures where the Hall crossover significantly interferes with the classical transition at T_N. The difference between the crossed-field and single-field results might arise from differently strong classical fluctuations. They are presumably strongly enhanced for the crossed-field orientation with the field in the magnetic easy plane, as here the magnetization is one order of magnitude larger compared to the single-field orientation. Finally, we note that within experimental accuracy the data are well described over the complete range 18 mK $\leqslant T \leqslant$ 1 K by a proportionality to temperature. This implies a vanishing width at $T \to 0$ meaning that the crossover becomes infinitely sharp in the zero temperature limit, with such an abrupt change suggesting a sudden reconstruction of the Fermi surface at the QCP.

Finally, for a full characterization of the crossover in the Hall coefficient we examine its height. The limiting values of the crossover in the linear-response Hall coefficient, i.e., R_H^0 and R_H^∞ are plotted in figure 6(a). For a proper evaluation we first analyze the low temperature behavior of the measured initial-slope Hall coefficient in zero tuning field, i.e., $R_H\ (T, B_2 = 0)$. The representation against T^2 in figure 6(a) reveals a quadratic temperature dependence, setting in just below the Néel temperature, as previously observed for the electrical resistivity [16]. Such a quadratic temperature dependence of the Hall coefficient is likely to arise from finite temperature corrections within a Fermi-liquid description. An enhancement, as for the corresponding term in the resistivity, might render this term observable in heavy-fermion materials. In fact, we observe a quadratic temperature dependence of R_H not only in the magnetically ordered phase, but also in the field induced Fermi-liquid state of $YbRh_2Si_2$ and in the paramagnetic ground state of the heavy-fermion material $YbIr_2Si_2$, as shown in figures 6(d) and (e). The quadratic form of $R_H(T)$ is limited to the regime where also resistivity obeys a quadratic temperature dependence.

As a next step we compare the zero-field Hall coefficient R_H^0 extracted from the analysis of the crossover with the truly measured zero-field ($B_2 = 0$) Hall coefficient. This comparison is non-trivial, as R_H^0 was allowed to vary during the fitting procedure. Nevertheless, we find a perfect agreement, proving the consistency of our analysis. Consequently, we can utilize the power law found for $R_H(T)$ to extrapolate R_H^0 to zero temperature. This is highlighted by the solid lines in

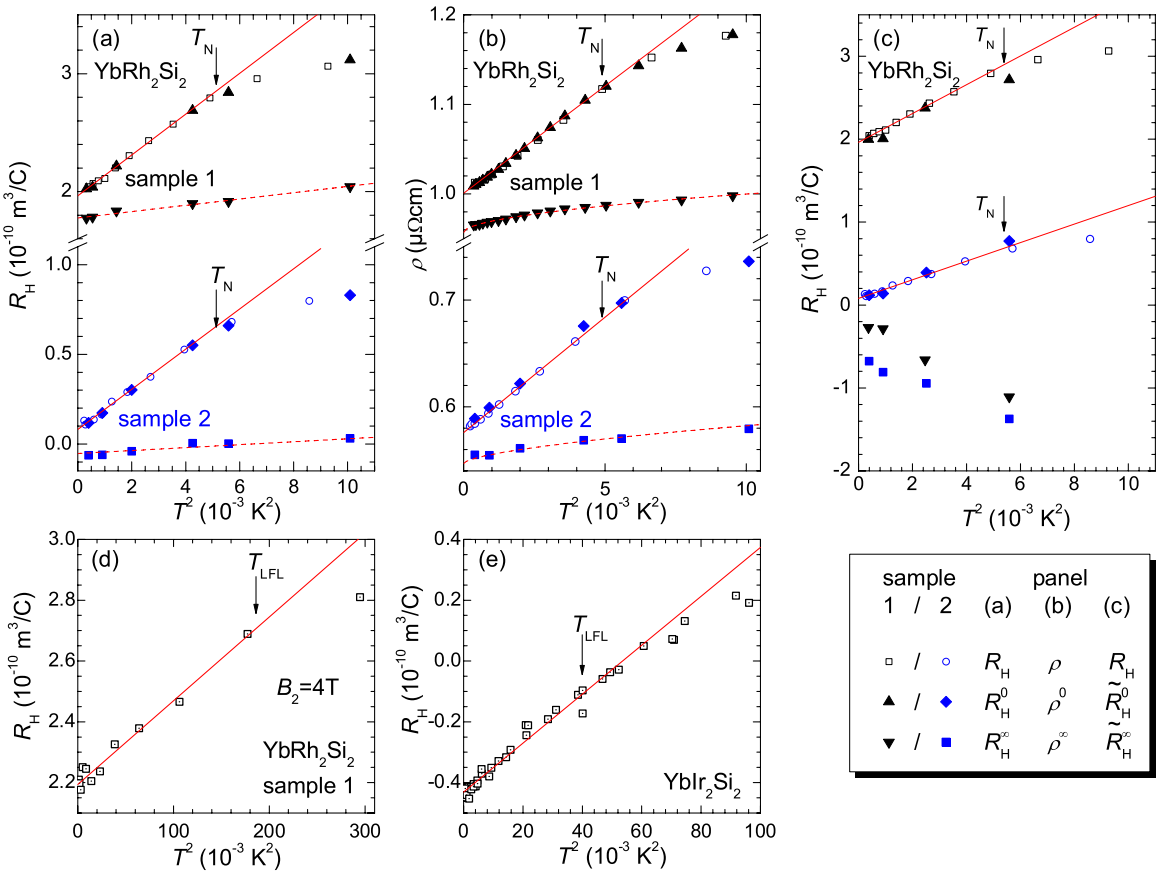

Figure 6. Low temperature behavior of the Hall coefficient and resistivity. (a) The initial-slope Hall coefficient is plotted against temperature squared. The zero-field Hall coefficient R_H^0 and high-field Hall coefficient R_H^∞ extracted from the fits to the field dependence of the linear-response Hall coefficient are included (cf figure 2). (b) Resistivity of both $YbRh_2Si_2$ samples, together with the zero-field value ρ^0 and ρ^∞ extracted from the fits to the magnetoresistivity (figures 3(c) and (d)). (c) Analog parameter of the differential Hall coefficient: $\tilde{R}_H^0$ and $\tilde{R}_H^\infty$ are plotted against T^2, together with the initial-slope Hall coefficient for both samples. Arrows in (a)–(c) mark the Néel temperature. (d) Initial-slope Hall coefficient of $YbRh_2Si_2$ against T^2 measured at a constant tuning field $B_2 = 4$ T, i.e., in the field induced Fermi-liquid state. (e) Hall coefficient of $YbIr_2Si_2$ against T^2. Arrows in (d) and (e) mark the Fermi-liquid temperature below which the resistivity obeys a quadratic temperature dependence [2, 19]. Solid lines in (a)–(e) represent fits of a quadratic temperature dependence to the data. Dashed lines are a guide to the eye.

figure 6(a). The evolution of R_H^0 is to be compared with that of the high-field value R_H^∞. A distinct power law cannot be established for R_H^∞ due to the limited statistics. Nevertheless, the fact that R_H^∞ features only a small temperature dependence allows a proper extrapolation of this parameter, as indicated by the dashed lines in figure 6(a). Importantly, the finite difference between R_H^0 and R_H^∞ persists down to zero temperature for both samples. Complementary conclusions can be derived for the parameters extracted from the analysis of the magnetoresistivity and differential Hall coefficient. In fact, ρ^0 and ρ^∞ plotted in figure 6(b) behave very similar to R_H^0 and R_H^∞. A quadratic form of $\rho(T)$ and $\rho^0(T)$ sets in just below T_N. Also, the high-field value ρ^∞ resembles the behavior of R_H^∞. On this basis a proper extrapolation of both ρ^0 and ρ^∞ yields a persistent finite difference in the limit of zero temperature. For the case of the differential Hall coefficient the zero-field value $\tilde{R}_H$ depicted in figure 6(c) follows the very same quadratic form of the initial-slope Hall coefficient as R_H^0, thus further proving the consistency of our analysis. The only difference between the crossed-field and single-field results affects the high-field values R_H^∞ and $\tilde{R}_H^\infty$. Whereas R_H^∞ is seen to increase with increasing temperature, $\tilde{R}_H^\infty$ decreases. In addition, the absolute values of both differ, $\tilde{R}_H^\infty$ appears to be reduced and negative for both samples, whereas R_H^∞ is only negative for sample 2 at the lowest temperatures. As a consequence, the difference $\tilde{R}_H^0 - \tilde{R}_H^\infty$ is larger than $R_H^0 - R_H^\infty$, reflecting the larger step height seen in the single-field experiment (compare figures 2, 3(a) and (b)). For the extrapolation of the parameters of the single-field experiment, we again take advantage of the quadratic form for $\tilde{R}_H^0$ and the smooth evolution of $\tilde{R}_H^\infty$. As for the crossed-field results, the finite difference $\tilde{R}_H^0 - \tilde{R}_H^\infty$ persists in the zero-temperature limit. In summary, the difference between the zero-field value and the high-field value of the crossover in all three quantities remains finite down to zero temperature for both samples. Together with the vanishing FWHM and the position of the crossover converging to the QCP, this difference marks a finite jump of the Hall coefficient. Consequently, the data strongly suggest that the Fermi surface

undergoes a severe reconstruction at the QCP. The difference between R_H^0 and R_H^∞ is associated with the different Fermi surfaces of the different adjacent ground states (cf [13]).

We can rule out that the discontinuity of R_H at the QCP originates from a change in scattering rates only. In fact, a slight shift in the balance of scattering rates for the two dominant bands is invoked to explain the strong sample dependences of the background contribution in R_H. The sample dependences in $R_H(T)$ arise for different samples with minute differences in composition and different values of disorder. However, the (extrapolated) jump in R_H across the QCP is a property associated with criticality; moreover, it occurs as a function of a continuous variation of the control parameter—the magnetic field—at a continuous phase transition. In fact, magnetostriction measurements show that the phase transition remains continuous down to at least 15 mK [20]. Without a jump of Fermi surface, a change in R_H resulting from a variation of scattering rates *per se* across a continuous phase transition must be continuous with respect to the control parameter and cannot have a jump across the QCP.

These strong indications for a Fermi surface reconstruction at the QCP in $YbRh_2Si_2$ provide the basis for the scaling analysis of the Hall crossover width. The linear-in-temperature form of the FWHM was found to point towards an E/T scaling of the critical fluctuations [14]. Our magnetoresistivity measurements establish the proportionality of the FWHM with temperature persists up to 1 K, i.e., over almost two decades. Consequently, these results underpin the conclusion of an unconventional QCP in $YbRh_2Si_2$.

4. Comparison with spin-density-wave quantum critical point

A canonical SDW QCP is realized in pure and V-doped Cr [21]. The evolution of the Hall coefficient across the pressure-driven QCPs has been systematically studied in both cases [22, 23], and is shown in figure 7 for the lowest measured temperatures. These temperatures (5 and 0.5 K for pure Cr and $Cr_{0.968}V_{0.032}$) are already small compared to the natural temperature scales of the system, yet the Hall coefficient is seen to be smoothly evolving as a function of the control parameter. Such a smooth evolution is expected theoretically [9, 24, 25]. The Fermi surface of a SDW state is reconstructed from that of the paramagnetic state through a band folding, which is more pronounced for a system such as Cr whose Fermi surfaces are nested. However, when the SDW order parameter is adiabatically switched off, the folded Fermi surface is smoothly connected to the paramagnetic one. As a result, the Hall coefficient does not show a jump, provided the nesting is not perfect [25].

In a magnetic field-driven QCP, the nonzero critical field can give rise to a small discontinuity in the magnetotransport coefficients, even in the case of an SDW QCP [26]. Approaching the QCP, the energy scale associated with the vanishing order parameter becomes smaller than the scale associated with the Lorentz force, leading to a non-linearity in the system's response to the Lorentz force, reflected in a breakdown of the weak-field magnetotransport. The linear

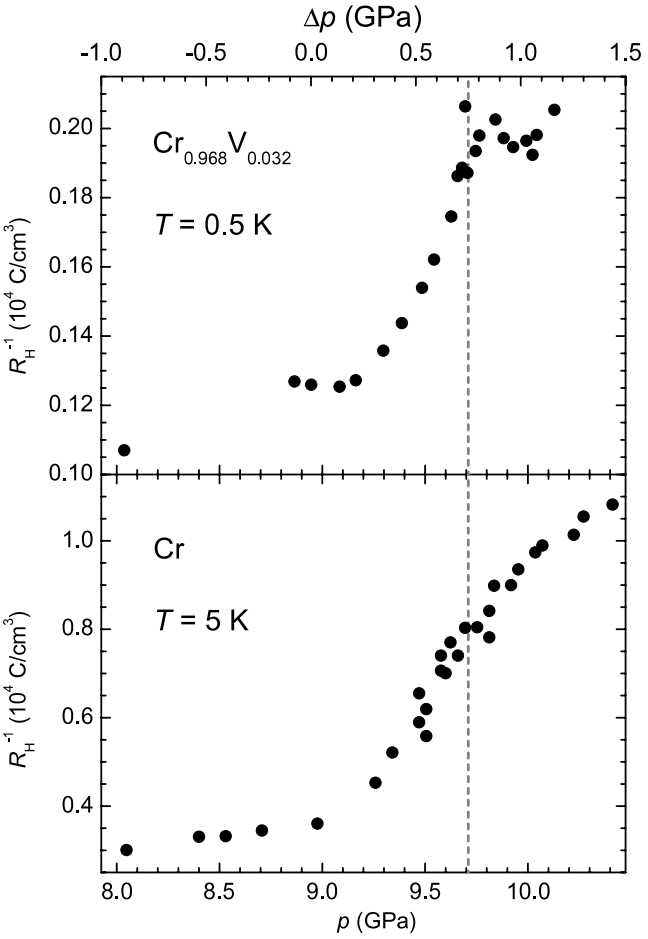

Figure 7. Inverse of the Hall coefficient of $Cr_{0.968}V_{0.032}$ (upper panel) and Cr (lower panel) as a function of pressure. In the upper panel, Δp is the external pressure for $Cr_{0.968}V_{0.032}$, and an effective pressure when the V-concentration differs from 0.032 [22]. In the lower panel, the result is shown only in the vicinity of the critical pressure [23], so that the two panels cover the same pressure extent. The dashed lines label the critical pressure.

field dependence of the magnetoresistance in $Ca_3Ru_2O_7$ was taken as an indication thereof [27]. More significantly, the breakdown of weak-field magnetotransport may lead to a jump in the Hall coefficient, which, however, does not appear to have been seen in any of the other quantum critical systems. This is not surprising, as the jump in the Hall coefficient is likely to be very small. In fact, for the case of the cuprates, mean field theory predicts that the anomaly in the Hall response at the critical doping level is non-observably small even though the SDW gap is large [28]. Disorder may smear the jump of the Hall coefficient into a smooth crossover.

As described above, in the pressure-driven SDW QCP of the V-doped and pure Cr [22, 23], the Hall coefficient (and the resistivity) is smooth across the QCP, with a crossover width that does not track with the strength of disorder (figure 7), in contrast to the scenario of a breakdown of the weak-field limit. For the field-driven QCP of $YbRh_2Si_2$, the issue of nonlinear response to the Lorentz force is completely avoided by the crossed-field Hall setup, in which the Lorentz field B_l

can be vanishingly small while the tuning field B_2 is fixed at its critical value. As seen in figure 1, the Hall resistivity is indeed linear in B_1, even at the critical B_2. Our conclusion is reinforced by considerations of several other factors. Our measured width of the critical crossover component is the same for both samples (1 and 2) that have different amounts of disorder (figure 5). The fact that the single-field Hall coefficient and magnetoresistivity have the same crossover width as the crossed-field Hall coefficient implies that, even in our single-field measurements, the critical Hall crossover does not originate from the above-noted nonlinear effect. This last conclusion is not surprising, given that at the critical B_{c1} field, $\omega_c\tau$ is of the order of 0.01 and 0.002 for samples 1 and 2 respectively.

5. Conclusion

Our study of the Hall effect and magnetoresistivity on the model system $YbRh_2Si_2$ provides a systematic characterization of the signatures of unconventional quantum criticality in this material. We analyze various magnetotransport properties for samples of different quality. We find a robust crossover in the Hall coefficient and magnetoresistivity on top of a sample dependent background. The crossover sharpens towards a finite jump at the QCP in the extrapolation to zero temperature, indicating a collapse of the Fermi surface. The relevance of such a Fermi surface reconstruction for the concept underlying our understanding of quantum critical metals cannot be overstated. Given the continuous nature of the transition, the collapse indicates that the Fermi surface is much more fragile than expected. Hence, it is necessary to introduce a new class of quantum phase transitions in metals. We also argue that our results are very different from the expectations for and observations in SDW QCPs.

Acknowledgments

Fruitful discussions with P Gegenwart, T Rosenbaum, A J Schofield and P Wölfle, as well as partial support by the DFG Research Group 960 'Quantum Phase Transitions' are acknowledged. SP acknowledges funding from the European Research Council under the European Community's Seventh Framework Programme (FP7/2007-2013)/ERC grant agreement no 227378. SK and QS were supported by the NSF Grant No. DMR-1006985 and the Welch Foundation Grant No. C-1411 and SF was partially supported by the Alexander von Humboldt foundation.

References

[1] Focus 2008 *Nat. Phys.* **4** 167–204
[2] Gegenwart P, Si Q and Steglich F 2008 *Nat. Phys.* **4** 186–97
[3] Hertz J A 1976 *Phys. Rev.* B **14** 1165–84
[4] Millis A J 1993 *Phys. Rev.* B **48** 7183–96
[5] Moriya T and Takimoto T 1995 *J. Phys. Soc. Japan* **64** 960–9
[6] Sachdev S 1999 *Quantum Phase Transitions* (Cambridge: Cambridge University Press)
[7] Schröder A *et al* 2000 *Nature* **407** 351–5
[8] Si Q, Rabello M S, Ingersent K and Smith J L 2001 *Nature* **413** 804–8
[9] Coleman P, Pépin C, Si Q and Ramazashvili R 2001 *J. Phys.: Condens. Matter* **13** R723–38
[10] Senthil T, Sachdev S and Vojta M 2003 *Phys. Rev. Lett.* **90** 216403
[11] Paschen S *et al* 2004 *Nature* **432** 881–5
[12] Friedemann S *et al* 2008 *Physica* B **403** 1251–3
[13] Friedemann S *et al* 2010 *Phys. Rev.* B **82** 035103
[14] Friedemann S *et al* 2010 *Proc. Natl Acad. Sci. USA* **107** 14547–51
[15] Trovarelli O *et al* 2000 *Physica* B **281/282** 372–3
[16] Gegenwart P *et al* 2002 *Phys. Rev. Lett.* **89** 056402
[17] Fert A and Levy P M 1987 *Phys. Rev.* B **36** 1907–16
[18] Paschen S, Lühmann T, Wirth S, Trovarelli O, Geibel C and Steglich F 2005 *Physica* B **359–361** 44–6
[19] Hossain Z *et al* 2005 *Phys. Rev.* B **72** 094411
[20] Küchler R, Weickert F, Gegenwart P, Oeschler N, Ferstl J, Geibel C and Steglich F 2004 *J. Magn. Magn. Mater.* **272-276** 229–30
[21] Yeh A, Soh Y A, Brooke J, Aeppli G, Rosenbaum T F and Hayden S M 2002 *Nature* **419** 459–62
[22] Lee M, Husmann A, Rosenbaum T F and Aeppli G 2004 *Phys. Rev. Lett.* **92** 187201
[23] Jaramillo R, Feng Y, Wang J and Rosenbaum T F 2010 *Proc. Natl. Acad. Sci. USA* **107** 13631–5
[24] Norman M R, Si Q, Bazaliy Y B and Ramazashvili R 2003 *Phys. Rev. Lett.* **90** 116601
[25] Bazaliy Y B, Ramazashvili R, Si Q and Norman M R 2004 *Phys. Rev.* B **69** 144423
[26] Fenton J and Schofield A J 2005 *Phys. Rev. Lett.* **95** 247201
[27] Kikugawa N, Rost A W, Hicks C W, Schofield A J and Mackenzie A P 2010 *J. Phys. Soc. Japan* **79** 024704
[28] Lin J and Millis A J 2005 *Phys. Rev.* B **72** 214506